nature communications

Article

https://doi.org/10.1038/s41467-026-69588-6

Copper damascene process-based high-performance thin-film lithium tantalate modulators

Received: 26 August 2025

Accepted: 29 January 2026

Published online: 26 February 2026

Check for updates

Mengxin Lin[1,2], Zihan Li[1,2], Alexander Kotz[3], Hugo Larocque[1,2], Nikolai Kuznetsov[1,2], Jiale Sun[1,2], Yichi Zhang[1,2], Shuhang Zheng[1,2], Johann Riemensberger[1,2,4], Christian Koos[3] & Tobias J. Kippenberg[1,2]

The conversion between electrical and optical signals underpins modern optical communication systems and increasingly requires tight co-integration with electronics at short length scales. Photonic integrated circuits based on thin-film lithium tantalate has emerged as a promising electro-optic platform due to its large Pockels coefficient, low birefringence, low bias drift, and high power handling, yet its integration with standardized microelectronic processes remains limited. Here we show that incorporating the copper Damascene process into thin-film lithium tantalate modulators enables a scalable, electronics-compatible fabrication approach. The resulting devices exhibit approximately 10% lower microwave loss than conventional gold-electrode designs, while simultaneously supporting watt-level on-chip optical power handling and maintaining a stable quasi-static half-wave voltage from 1 Hz to 1 MHz, with a bias point drift of only 0.4 dB over a 15-hour period when operated at 1.75 mW on-chip optical power. High-speed transmission experiments demonstrate line rates of 416 Gbit/s (PAM4) and 540 Gbit/s (PAM8) below the 25% soft-decision forward-error-correction threshold. These results establish a practical route toward scalable chip-on-wafer integration of electro-optic modulators with microelectronic circuits.

Integrated electro-optic (EO) modulators provide a scalable platform for converting information between electrical and optical domains, serving as key building blocks for high-capacity optical communications[1–3] and emerging chip-to-chip interconnects[4,5]. Recent progress in thin-film lithium niobate and thin-film lithium tantalate photonics integrated circuits has transformed traditional bulk devices[6,7]. The adoption of a layered "on-insulator" structure, combined with improved etching techniques[8], enables strong optical confinement and allows electrodes to be placed closer to the waveguide, thereby enhancing modulation efficiency. This structure also facilitates velocity matching between optical and microwave signals, resulting in higher modulation bandwidths. However, as the electrode gap is reduced to achieve tighter optical confinement and stronger modulation, the currents in the signal line and ground plane become increasingly concentrated near the gap due to the electromagnetic proximity effect[9]. This enhanced current concentration increases the per-unit-length resistance of the transmission line, leading to higher microwave loss. The resulting loss limits further improvements in voltage-bandwidth performance. Employing electrodes with periodic microstructured "T-rails" mitigates the proximity effect by introducing a larger effective gap while preserving the electric-field distribution required for efficient modulation[10–13]. An alternative approach to

[1]Institute of Physics, Swiss Federal Institute of Technology Lausanne (EPFL), Lausanne, Switzerland. [2]Institute of Electrical and Micro Engineering, EPFL, Lausanne, Switzerland. [3]Institute of Photonics and Quantum Electronics (IPQ), Karlsruhe Institute of Technology (KIT), Karlsruhe, Germany. [4]Present address: Department of Electronic Systems, Norwegian University of Science and Technology (NTNU), Trondheim, Norway. e-mail: tobias.kippenberg@epfl.ch

reducing microwave loss replaces conventional gold electrodes with low-resistivity metals, such as copper, which has a resistivity approximately 24% lower than gold[14].

While continuous efforts have been made to extend the voltage-bandwidth performance of thin-film lithium niobate and lithium tantalate modulators[15,16], most reported devices remain stand-alone prototypes, requiring bulky electrical probes and external control electronics. Meanwhile, AI-based applications are driving an ever-growing demand for higher data throughput, lower latency, and improved energy efficiency in modern computing systems[17]. To meet these requirements, co-packaged optics (CPO) has emerged as a transformative technology that tightly integrates photonics and electronics[18]. Such integration reduces high-frequency signal degradation, reduces energy consumption, and enables large-scale system scalability. Among various integration approaches, three-dimensional (3D) integration, as illustrated in Fig. 1a, offers the shortest metal interconnects by vertically stacking photonic and electronic chips, thereby minimizing signal loss and improving overall efficiency[19]. While this stacking is typically achieved through flip-chip bonding using microbumps[20], the industry is transitioning toward hybrid copper-copper bonding[21]. In this approach, copper surfaces are directly joined through thermally activated diffusion, eliminating solder interfaces and thereby reducing parasitic effects. A key enabler of this transition is planarized copper metallization achieved via the copper Damascene process, already widely adopted in both microelectronics[22] and silicon photonics[23]. However, ferroelectric photonic platforms still rely on conventional gold electrodes, highlighting the need for further innovation to achieve fully integrated, high-performance photonic-electronic systems.

Here, we address this challenge by incorporating the copper Damascene process into the fabrication of lithium tantalate photonic integrated circuits (PICs). This approach leverages a mature, low-cost, and widely adopted method used for metallization in microelectronics and silicon photonics. Using this process, we demonstrate integrated

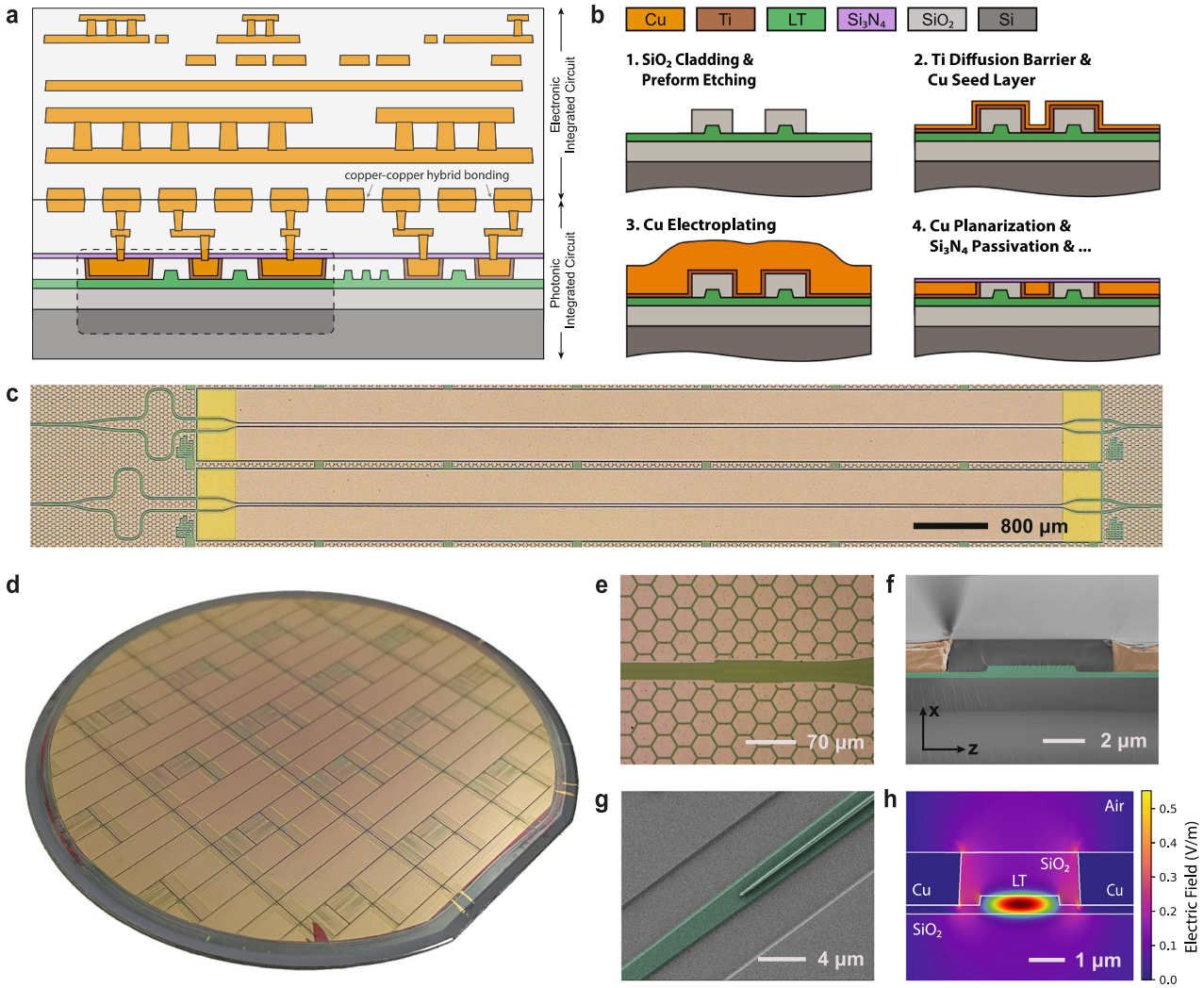

Fig. 1 | Copper Damascene process-based thin-film lithium tantalate Mach-Zehnder modulators. a Cross-section diagram illustrating the level of wiring enabled by the copper Damascene process in both electronic and photonic integrated circuits. The boxed region highlights the modulator architecture introduced in this work. **b** Simplified process flow for fabricating copper electrodes on patterned lithium tantalate wafers using a copper Damascene process. **c** Microscope image of two Mach-Zehnder modulators, each comprising two 1 × 2 multimode interference couplers, an unbalanced arm, and a pair of push-pull phase shifters. The yellow color indicates the gold-capped pads for stable and efficient electrode probing. Chip ID: D187_F1_C4. **d** A photograph of a manufactured 100-mm wafer hosting hundreds of copper Damascene lithium tantalate modulators on 50 dies. **e** Microscope image of a multimode interference coupler surrounded by honeycomb copper fillers, which are used to ensure uniform planarization. **f** Colored scanning electron microscopy image of the cross-section of the lithium tantalate waveguide (green) and copper electrodes (orange). **g** Colored scanning electron microscope image of a double-layer taper for efficient and broadband edge coupling between the chip and single-mode fibers. **h** Numerically simulated microwave and optical field distributions in the cross-section of the lithium tantalate modulator.

https://doi.org/10.1038/s41467-026-69588-6

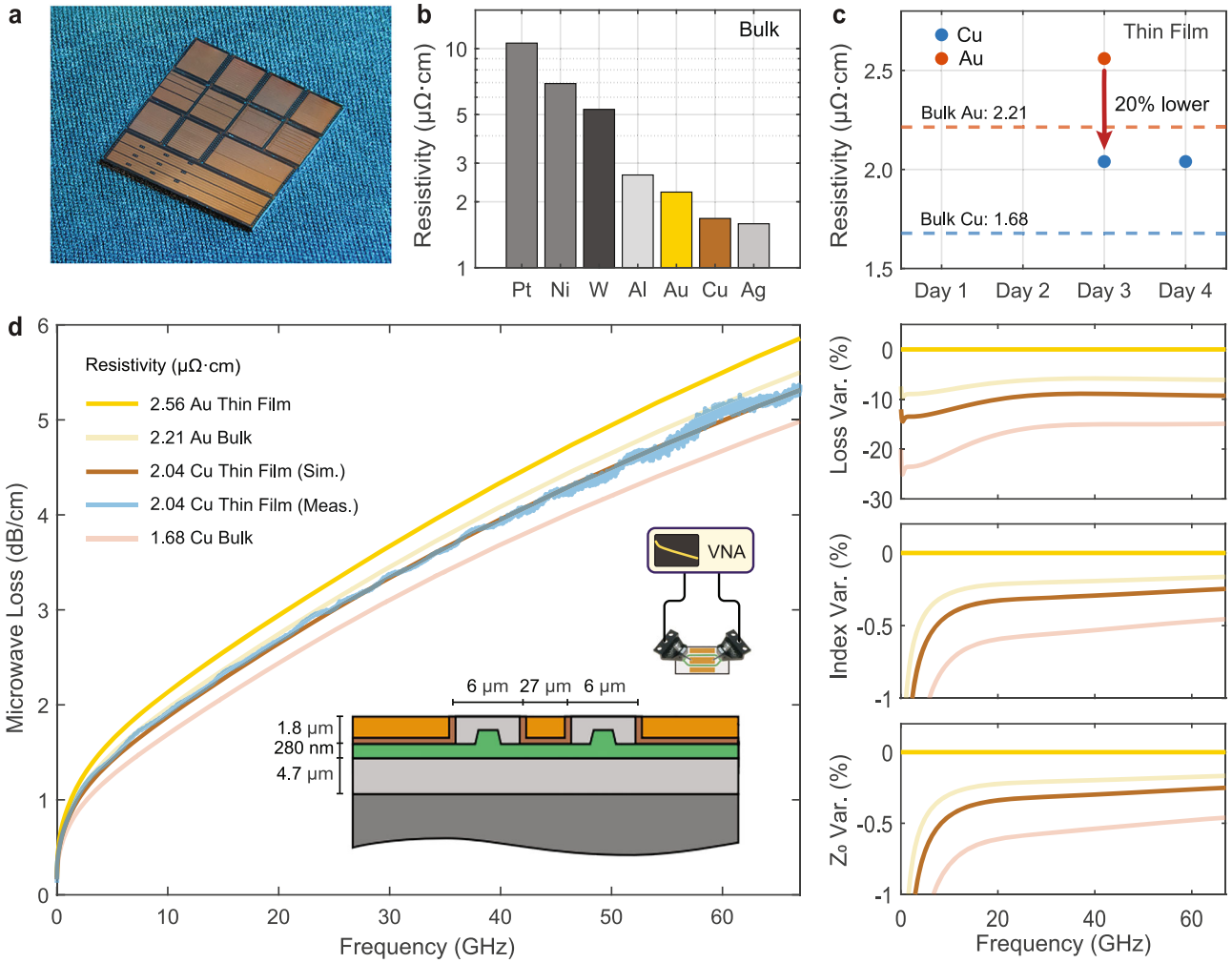

Fig. 2 | Electrical characterization of copper thin-film lithium tantalate modulators. a A photograph of copper Damascene coplanar waveguide electrode test structures fabricated on silicon. The smallest chip size is 5 mm × 5 mm. **b** Electrical resistivity of the seven most conductive elemental metals, sorted by decreasing bulk room-temperature resistivity. **c** Measured resistivity of thin-film gold and copper, and their evolution with time. The resistivity of the electroplated copper undergoes a 24% decrease within 48 h at room temperature due to its self-annealing effect, and is stabilized at 2.04 μΩ·cm, which is 20% lower than the measured resistivity of the thin-film gold. **d** Measured microwave losses for the fabricated copper coplanar waveguide electrodes, along with numerically simulated losses for electrodes composed of materials defined by different resistivities yet sharing the geometry of the fabricated device. Device ID: D187_F1_C7_1.06. Inset: microwave propagation loss testing apparatus and main dimensions used in the material stack of the measured device, as previously defined in Fig. 1a. Side panels: Corresponding percent loss, microwave effective index, and characteristic impedance (Z_0) variations of the simulated coplanar waveguide electrodes compared to thin-film gold.

electro-optic modulators with microwave losses approximately 10% lower than those employing conventional gold electrodes, while preserving the intrinsic benefits of thin-film lithium tantalate, including low optical loss, high modulation efficiency, and broad modulation bandwidth. The resulting planar electrode surface also supports direct chip-on-chip and chip-on-wafer bonding with driver electronics.

Fabrication

The devices were fabricated from a commercially available X-cut thin-film lithium tantalate (TFLT) wafer (NANOLN), which consists of 600 nm of lithium tantalate ($LiTaO_3$, LT), 4.7 μm of SiO_2, and a 525 μm-thick high-resistivity silicon substrate. The TFLT PICs were manufactured using an etching technique based on a diamond-like carbon hard mask, which can reliably produce both lithium niobate and lithium tantalate PICs[8,24]. The etch depth of the LT was 320 nm, leaving a 280 nm-thick slab for efficient electro-optic modulation and proper phase matching between microwave and optical signals.

Next, the copper Damascene process, outlined in Fig. 1b, was introduced to fabricate traveling-wave electrodes. This Damascene process differs from silicon nitride Damascene methods[25], which reduce optical propagation losses in waveguides, whereas we apply it to copper electrodes to minimize microwave loss. In this process, dielectric trenches are patterned and filled by electroplated copper, followed by chemical-mechanical polishing (CMP). This process produces well-defined electrodes with a smooth surface, potentially suitable for chip-on-wafer bonding. Further information on the fabrication is available in the "Methods". Figure 1c shows two fabricated Cu-TFLT MZMs extending over an effective modulation length of 6 mm. Figure 1d illustrates the fabricated 4-inch wafer with hundreds of Cu-TFLT MZMs, highlighting its potential for scalable integration of next-generation photonic systems. To improve the wafer's uniformity following the CMP process, inactive regions feature a filler copper pattern, which is visible in Fig. 1c–e. As shown in Fig. 1e–g, each modulator consists of 50:50 1 × 2 multimode interference (MMI) couplers, EO phase shifters operating in a push-pull configuration, and double-layer tapers for enhanced PIC-to-fiber coupling efficiency[26] (Fig. S1). As illustrated in Fig. 1f, the tight confinement of the modulator's microwave and optical modes

https://doi.org/10.1038/s41467-026-69588-6

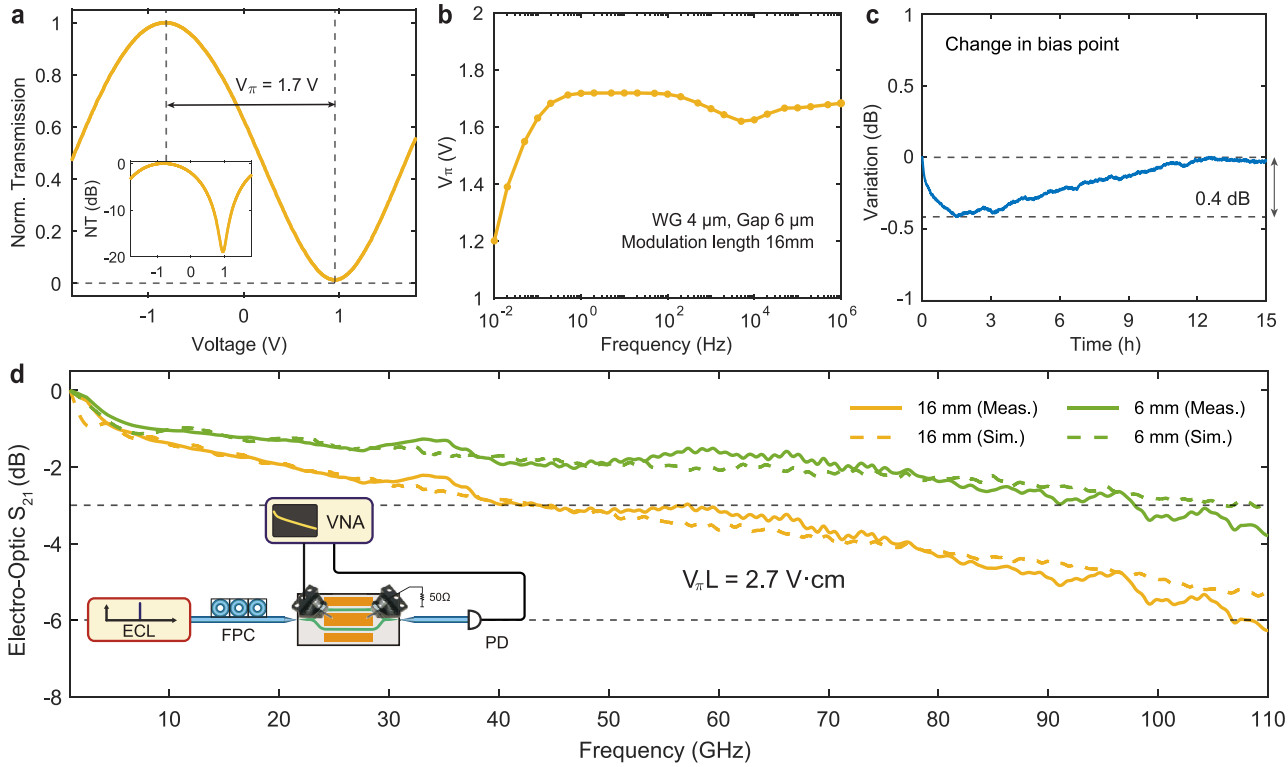

Fig. 3 | Electro-optic characterization of copper Damascene thin-film lithium tantalate Mach-Zehnder modulators. a Normalized optical transmission of a modulator as a function of the applied voltage, yielding a V_π value of 1.7 V. The device features a 16 mm modulation region with a 4 μm-wide waveguide width, and a 6 μm electrode gap. Device ID: D187_F6_C4_1.06. Inset: transmission plotted on a dB scale, showing a 20 dB extinction ratio. NT: Normalized Transmission. **b** Measured V_π as a function of the sweeping frequency of the applied voltage signal. **c** Long-term bias-point stability over 15 h for a device with a 6 mm modulation length, measured with an on-chip power of 1.75 mW. **d** Small-signal electro-optic response of devices with a modulation length of 16 mm (D187_F6_C6_1.02) and 6 mm (D187_F6_C4_1.06), respectively. Inset: testing apparatus for the electro-optic response measurement.

ensures strong overlap between the two fields and thus enhanced modulation efficiency.

Electrical transmission

To assess the potential of copper as an electrode material for high-performance modulators, we characterized the electrical properties of fabricated copper Damascene CPWs, including resistivity and microwave performance, and compared them with their conventional gold-based counterparts. Figure 2a shows a photograph of the test structures. For context, Fig. 2b presents the bulk resistivity of the seven most conductive elemental metals commonly used in microelectronics and photonics. Although thin films are typically employed in these applications, their resistivity depends on thickness and fabrication process; thus, bulk values are used here for a general comparison. Silver (1.59 μΩ·cm) exhibits the lowest resistivity, followed by copper (1.68 μΩ·cm), which is only 5.6% higher, and gold (2.21 Ω·cm), which is 39% higher[27]. We focus on copper and gold due to the impracticality of using silver (see Discussion). Figure 2c compares the measured resistivity of thin-film gold and copper and its evolution with time. The gold thin film (796 nm) was deposited by electron beam evaporation, and the copper thin film (1170 nm) by electroplating. Both were formed on silicon carrier wafers with a 2 μm silicon dioxide layer and characterized using a four-point probe and mechanical profilometry. The electroplated copper exhibited a 24% decrease in resistivity within 48 h at room temperature due to self-annealing[28], stabilizing at 2.04 μΩ·cm - approximately 20% lower than that of gold. Studies suggest that the resistivity of electroplated copper could be further reduced to 1.77 μΩ·cm[29] via process optimization. Using these measured values, we modeled the microwave behavior of the fabricated CPWs through full-wave electromagnetic simulations (Fig. S2). Figure 2d shows the simulated microwave loss of a 16 mm-long copper Damascene CPW with a 6 μm gap and a 27 μm signal line, alongside simulated CPWs with varying resistivities but identical geometries. The measured microwave loss agrees well with the simulation, validating the model. The data indicate that copper electrodes yield approximately 10% lower microwave loss than gold, while the propagation index and characteristic impedance change by less than 0.3%. The dependence of the microwave effective index on design parameters is provided in Fig. S3.

Electro-optic modulation

A direct approach to assess the modulators' performance is to measure their EO response, including the quasi-static half-wave voltage (V_π) and the 3 dB EO bandwidth. Finite-element simulations (COMSOL Multiphysics) were performed to analyze the $V_\pi L$ product and optical loss for various modulator geometries. A design with 6 μm electrode gap and a 4 μm-wide waveguide was selected. This relatively wide waveguide maintains a similar $V_\pi L$ and optical loss while allowing a larger electrode gap that reduces microwave loss (Fig. S4)[30]. A 100 μm-long adiabatic linear taper connects the modulation region to the single-mode routing waveguide, ensuring single-mode operation. The quasi-static V_π was measured by applying a low-frequency triangular voltage signal to the CPW electrode and recording the optical output simultaneously. Figure 3a shows the normalized transmission of a modulator as a function of the applied voltage, linearly swept at 100 Hz, exhibiting a near-sinusoidal response with a V_π of 1.7 V. For a device length of 16 mm, this corresponds to a $V_\pi L$ of 2.7 V·cm, closely matching the simulated value of 2.64 V·cm. The inset dB-scale plot shows an extinction ratio of 20 dB, suitable for advanced modulation formats such as PAM4 and PAM8. The dependence of the V_π on the modulation frequency was also examined. As shown in Fig. 3b, V_π

remains stable across a wide frequency range from 1 Hz to 1 MHz. More detailed results are shown in Fig. S5. Similar measurements were performed over a range of on-chip optical powers up to 1.17 W, and the results are shown in Fig. S6. This flat frequency response contrasts with the pronounced low-frequency instability previously reported for lithium niobate modulators with gold CPWs[31]. A small fluctuation (< 0.1 V) in V_π between 1 kHz and 100 kHz is attributed to dielectric relaxation intrinsic to the Cu–$LiTaO_3$ stack. Such effects arise from slow polarization dynamics or charge trapping in the ferroelectric layer when the modulation frequency approaches the characteristic relaxation rate. The magnitude and frequency of this fluctuation remain unchanged as the on-chip optical power increases from 1 mW to 1.17 W, confirming that it is not due to optical intensity-dependent photorefractive effects. As indicated by the stable quasi-static V_π, the modulator exhibits excellent long-term stability, showing only a 0.4 dB bias drift over 15 h at 1.75 mW on-chip power (Fig. 3c). This stability removes the need for active thermal biasing and its associated power-hungry heaters[30]. More detailed bias-drift measurement results are provided in Fig. S7. Figure 3d presents the measured EO response up to 110 GHz. The 3 dB EO bandwidth reaches 40 GHz for a 16 mm-long device and 100 GHz for a 6 mm-long device, both with a 6 µm electrode gap. The simulated EO response is derived from the measured electrical response and agrees well with the experimental data, validating the measurement. Simulations further indicate that the 3-dB EO bandwidth is approximately 10% higher than that of comparable gold-electrode devices (Fig. S8). These results demonstrate that the copper-electrode-based modulators combine high EO bandwidth with low drive voltage, enabling high-speed optical communication applications.

Optical communications

To demonstrate the exceptional performance of our Cu-TFLT MZM, we performed a high-speed intensity-modulation and direct-detection (IMDD) signaling experiment. The experimental apparatus for this task is illustrated in Fig. 4a and further described in the "Methods". We generated and received PAM4 and PAM8 data signals with symbol rates between 144 GBd and 208 GBd. Figure 4b displays the measured bit error ratios (BER) of the various PAM signals as a function of symbol rate. The horizontal dashed lines indicate the thresholds for typical soft-decision (SD) forward-error correction (FEC) with 25% and 15% overhead, and for hard-decision (HD) FEC with 7% overhead. The results show that we can transmit 180 GBd PAM8 signals and 208 GBd PAM4 signals while the respective BERs of 3.76×10^{-2} and 3.56×10^{-2} are still below the 25% SD-FEC limit. In Fig. 4c, we further calculate the generalized mutual information (GMI) of our measurements based on log-likelihood ratios by using an additive white Gaussian noise channel model[32]. The dashed curves depict the achievable information rate (AIR), which is the product of the GMI and the symbol rate. The solid curves in Fig. 4c show the net data rates for measurements with BER below the 25% SD-FEC limit, where the net data rates are determined by multiplying the transmitted line rates by the code rate that is associated with the normalized GMI threshold, extracted from[33]. The results indicate that the highest AIR of 449 Gbit/s is achieved by using PAM8 signals at a symbol rate of 176 GBd. This corresponds to a net data rate of 423 Gbit/s, which is on par with results demonstrated for high-bandwidth thin-film lithium niobate MZMs[34]. Comparison of these data rates and other metrics achieved in this work, along with those from other state-of-the-art lithium niobate and lithium tantalate modulators, is available in Table S1. It should be noted that some of the results, such as the PAM4 symbol rate, were limited by the bandwidth of our driver electronics, not by the MZM itself.

Discussion

From a materials perspective, metals with lower resistivity reduce microwave loss. Gold electrodes are conventionally used in bulk lithium niobate modulators due to their relatively low resistivity, chemical stability, and ease of fabrication by evaporation and lift-off or electroplating followed by etching[35,36]. With the emergence of thin-film platforms and growing demands for high-speed data connectivity, replacing conventional gold electrodes with copper Damascene electrodes has become strategically important. Copper offers lower resistivity, improved voltage-bandwidth performance, and compatibility with scalable electronic integration[22,23]. Although silver has slightly lower resistivity than copper, it suffers from diffusion and sulfidation issues that cannot be addressed as effectively as in the case of copper[37,38]. Moreover, silver's electroplating and CMP processes are less mature. Consequently, despite its marginal electrical advantage, silver is less reliable and less cost-effective for large-scale integration.

To assess the stability of our copper Damascene electrodes, we measured their microwave performance over an extended period and conducted thermal cycling tests. The results show that the electrodes maintained their propagation loss and effective index over six months of ambient storage (Fig. S9). These properties also remained unchanged under a 45-minute-per-cycle thermal cycling test between room temperature and 80 °C (Fig. S10). We further characterized the microwave metrics and quasi-static V_π values on devices from nine fields across a 4-inch wafer (Fig. S11). The results show that the device-to-device variation of the electrical S_{21} parameter is below 0.1 dB at 60 GHz (less than 3% in linear scale), the microwave group indices are all well matched to the optical group index of 2.22 within a tolerance of ± 0.03, and the quasi-static V_π varies by less than 5%. These results confirm high process reproducibility and support the scalability of our approach.

Further improvements in the voltage-bandwidth performance could be achieved by adopting a microstructured electrode design[10–13]. Test structures fabricated with the copper Damascene process demonstrate the potential to reduce microwave loss to 2–4 dB/cm, while preserving velocity and impedance matching through proper design parameters (Fig. S12). In addition, the copper Damascene process can reliably produce submicrometer-scale features, which is difficult to achieve using the conventional lift-off process. To accommodate the higher microwave effective index of these designs, the thickness of the buried oxide layer may need further optimization[39].

We also envision a full co-packaging of Pockels modulators with their driving circuits using emerging copper-copper hybrid bonding techniques[21]. Although a full bonding demonstration is beyond the scope of this study, we have shown morphological results that strongly support the feasibility of chip-on-wafer integration using our process. Specifically, the CMP-treated copper electrodes exhibit an RMS roughness below 11 nm and a maximum step height of approximately 37 nm at the Cu-SiO_2interface (Fig. S13), values that fall within accepted limits for hybrid bonding[40].

In summary, our results directly demonstrate the advantages of implementing a copper Damascene process for electro-optic modulators targeting high-bandwidth telecommunications, while also showing strong potential for co-integration with high-speed microelectronics.

Methods

Copper damascene fabrication flow

To begin with, the TFLT PICs were cladded with a 2.5 µm-thick silicon dioxide layer by plasma-enhanced chemical vapor deposition (PECVD). This cladding layer will embed the subsequently formed copper electrodes. The layout for these electrodes was defined with a DUV stepper lithography (ASML PAS 5500/350C) and transferred as preforms into the cladding layer through fluorine-based dry etching in a reactive ion etcher. These preforms were coated with 10 nm of titanium (Ti) and 100 nm of copper (Cu) through sputtering (Alliance-Concept DP 650). The titanium layer serves as a barrier to prevent copper from diffusing

https://doi.org/10.1038/s41467-026-69588-6

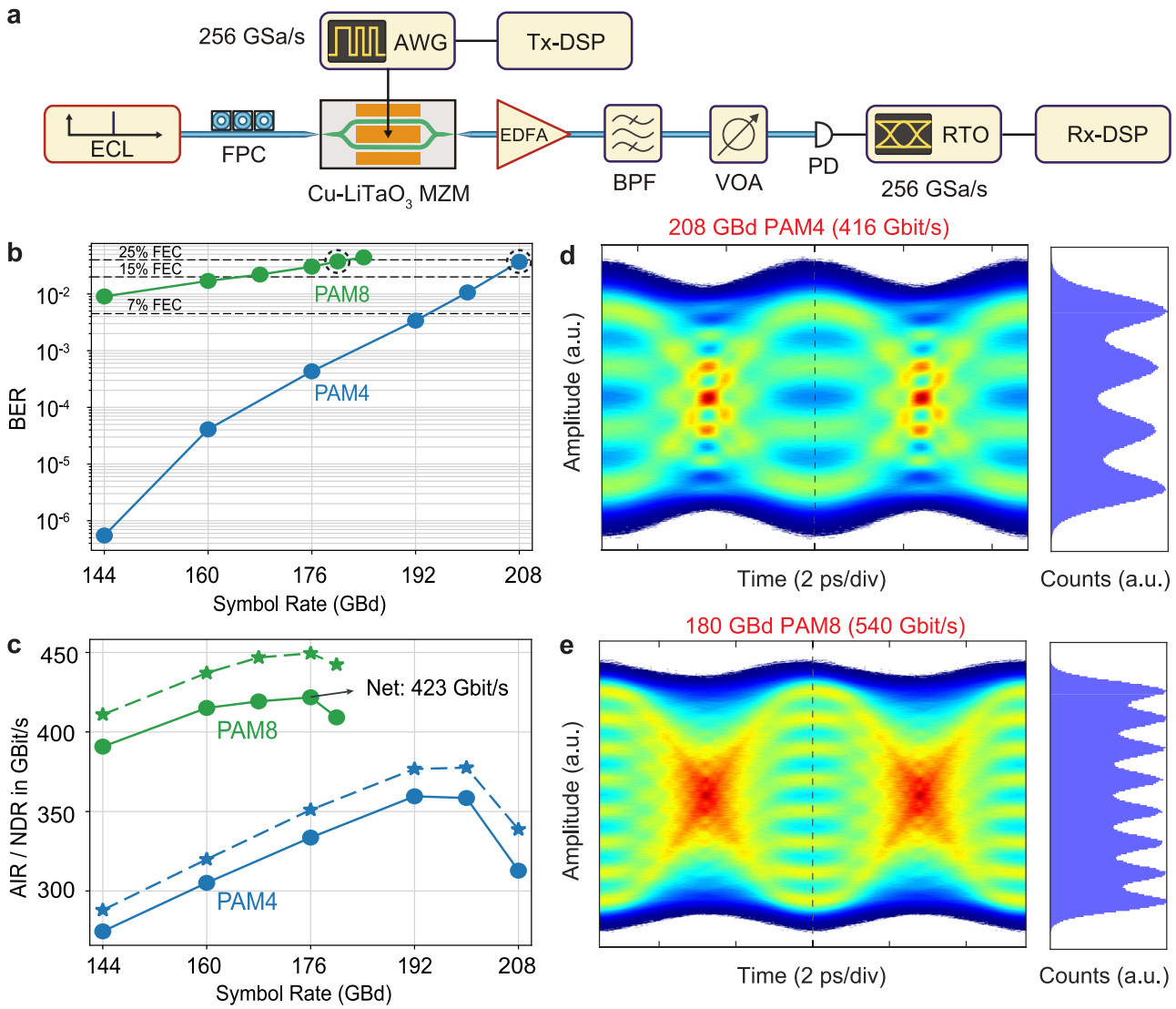

Fig. 4 | Data transmission experiment using intensity-modulation direct detection with a copper Damascene thin-film lithium tantalate modulator. **a** An experimental apparatus: an external cavity laser (ECL) is used as the light source, and a fiber polarization controller (FPC) adjusts the polarization state of the light. Optical input and output coupling to the lithium tantalate modulator (D187_F6_C4_1.06) is achieved using a pair of lensed fibers. The drive signals are synthesized by transmitter digital signal processing (Tx-DSP) and generated by an arbitrary waveform generator (AWG). The modulated optical signal is amplified using an erbium-doped fiber amplifier (EDFA), and out-of-band amplified spontaneous emission (ASE) noise is suppressed by a tunable bandpass filter (BPF). The amplified signal then passes through a variable optical attenuator (VOA) before being detected by a photodiode (PD). A high-speed real-time oscilloscope (RTO) samples the resulting signal, which is processed offline by receiver DSP (Rx-DSP). **b** Measured bit error ratios (BER) as a function of symbol rate for PAM8 (green) and PAM4 (blue) signals. The horizontal black dashed lines denote the thresholds for 25% and 15% soft-decision forward error correction (SD-FEC), as well as 7% hard-decision forward error correction (HD-FEC). **c** Extracted available information rates (AIR, dashed lines) and corresponding net data rates (NDR, solid lines) for measurements with BER values below the 25% SD-FEC threshold. The maximum NDR of 423 Gbit/s is obtained by using a PAM8 signal at a symbol rate of 176 GBd. **d**, **e** Eye diagrams and corresponding histograms, taken at the center of the symbol slot (indicated by the vertical dashed line), for the circled data points marked in (**b**).

into the surrounding dielectric[41]. It also provides adhesion to a subsequently sputtered copper layer, acting as a seed to facilitate copper electroplating. The electroplating was performed in a Silicet Electroplating unit and contributed to a 2.8 µm thick copper layer with low resistivity (2.04 µΩ·cm). Chemical mechanical planarization (CMP) was employed to remove the excess copper, leaving copper only in the etched preforms with a final thickness of 1.8 µm. This relatively thick metal layer minimizes microwave losses in the CPW electrodes across frequencies ranging from tens of GHz to 110 GHz (Fig. S14). Since the electrodes are embedded within a SiO_2 cladding layer and share a common top surface, their thickness can be indirectly monitored by measuring the thickness of nearby SiO_2 windows using spectroscopic reflectometry, as shown in Fig. 1c. Subsequently, a 100 nm-thick silicon nitride passivation layer was deposited with PECVD to prevent copper oxidation. The electrode pads were then opened and capped with gold (Au) for efficient and stable electrical probing. Finally, chip singulation was achieved through a combination of dry etching—standard reactive ion etching for LT and silicon dioxide, deep reactive ion etching for silicon, and backside grinding. This process ensures smooth facets for edge coupling to single-mode fibers.

Data transmission apparatus

An external-cavity laser (ECL, 17.8 dBm at 1550 nm) provides the optical carrier. A high-speed arbitrary-waveform generator (AWG, M8199B, Keysight) is used to generate the electrical drive signal, which is fed to the CPW of the MZM via a 20 cm-long RF cable, a broadband RF

amplifier, and a 110 GHz RF probe. We synthesize various pulse-amplitude modulation (PAM) signals based on pseudo-random bit sequences and apply root-raised cosine pulse-shaping filters with a roll-off of $\beta = 0.05$. We account for the frequency-dependent RF loss up to the input of the feeding probe by applying a linear minimum-mean-square-error (MMSE) predistortion. The CPW is terminated by a 50 Ω resistor via a second 110 GHz RF probe. As previously demonstrated in Fig. 3c, the EO stability of the Cu-TFLT modulator allows reliable DC biasing at the quadrature point for intensity modulation with a bias-T attached to the second probe. The optical power at the output fiber of the MZM operated at the quadrature point is 5.6 dBm, which exceeds the power requirements in typical specifications for high-speed optical Ethernet transceivers[42]. Still, an additional erbium-doped fiber amplifier (EDFA) was needed in the experiment to reach sufficient power levels for the high-speed photodiode (8.5 dBm) at the receiver. Note that a practical transceiver implementation could rely on a sufficiently broadband amplifier after the photodiode, thereby rendering the EDFA unnecessary. In our experiments, the out-of-band amplified spontaneous-emission (ASE) noise of the EDFA is suppressed by a tunable bandpass filter (BPF), and a variable optical attenuator (VOA) is used to adjust the power level of 8.5 dBm at the input of the photodiode. The electrical signal at the photodiode output is digitized by a real-time oscilloscope (RTO, UXR 1004A, Keysight) with an analog bandwidth of 105 GHz and a sampling rate of 256 GSa/s. The data is finally extracted by an offline receiver DSP (Rx-DSP), which contains resampling to 2 Sa/symbol, timing recovery, linear Sato equalization, and an additional decision-directed least-mean-square (DD-LMS) equalizer.

Data availability

The experimental datasets and scripts used to produce the plots in this paper are available at Zenodo (https://zenodo.org/records/18185066).

References

1. Koenig, S. et al. Wireless sub-THz communication system with high data rate. *Nat. Photonics* **7**, 977–981 (2013).
2. Marin-Palomo, P. et al. Microresonator-based solitons for massively parallel coherent optical communications. *Nature* **546**, 274–279 (2017).
3. Rizzo, A. et al. Massively scalable Kerr comb-driven silicon photonic link. *Nat. Photonics* **17**, 781–790 (2023).
4. Sun, C. et al. Single-chip microprocessor that communicates directly using light. *Nature* **528**, 534–538 (2015).
5. Atabaki, A. H. et al. Integrating photonics with silicon nanoelectronics for the next generation of systems on a chip. *Nature* **556**, 349–354 (2018).
6. Wang, C. et al. Integrated lithium niobate electro-optic modulators operating at CMOS-compatible voltages. *Nature* **562**, 101–104 (2018).
7. He, M. et al. High-performance hybrid silicon and lithium niobate Mach-Zehnder modulators for 100 Gbit s-1 and beyond. *Nat. Photonics* **13**, 359–364 (2019).
8. Li, Z. et al. High density lithium niobate photonic integrated circuits. *Nat. Commun.* **14**, 4856 (2023).
9. Mei, S. & Ismail, Y. I. Modeling skin and proximity effects with reduced realizable rl circuits. *IEEE Trans. Very Large Scale Integr. (VLSI) Syst.* **12**, 437–447 (2004).
10. Bennion, I. & Walker, T. Guided-wave devices and circuits. *Phys. World* **3**, 47 (1990).
11. Spickermann, R. & Dagli, N. Experimental analysis of millimeter wave coplanar waveguide slow wave structures on GaAs. *IEEE Trans. Microw. Theory Techn.* **42**, 1918–1924 (1994).
12. Kharel, P., Reimer, C., Luke, K., He, L. & Zhang, M. Breaking voltage–bandwidth limits in integrated lithium niobate modulators using micro-structured electrodes. *Optica* **8**, 357–363 (2021).
13. Chen, G. et al. High-performance thin-film lithium niobate modulator on a silicon substrate using a periodic capacitively loaded traveling-wave electrode. *APL photonics* **7**, 026103 (2022).
14. Zhang, Y. et al. Systematic investigation of millimeter-wave optic modulation performance in thin-film lithium niobate. *Photon. Res.* **10**, 2380–2387 (2022).
15. Xu, M. et al. Dual-polarization thin-film lithium niobate in-phase quadrature modulators for terabit-per-second transmission. *Optica* **9**, 61–62 (2022).
16. Xu, M. et al. Attojoule/bit folded thin film lithium niobate coherent modulators using air-bridge structures. *Apl Photonics* **8**, 066104 (2023).
17. Goodfellow, I. et al. Generative adversarial networks. *Commun. ACM* **63**, 139–144 (2020).
18. Huang, J. Gtc 2025 keynote address. *NVIDIA*. (2025).
19. Xiang, C. & Bowers, J. E. Building 3d integrated circuits with electronics and photonics. *Nat. Electron.* **7**, 422–424 (2024).
20. Daudlin, S. et al. Three-dimensional photonic integration for ultra-low-energy, high-bandwidth interchip data links. *Nat. Photonics* **19**, 502–509 (2025).
21. Moore, S. K. The copper connection: Hybrid bonding is the 3D-chip tech that's saving Moore's law. *IEEE Spectr.* **61**, 34–39 (2024).
22. Andricacos, P. C., Uzoh, C., Dukovic, J. O., Horkans, J. & Deligianni, H. Damascene copper electroplating for chip interconnections. *IBM J. Res. Dev.* **42**, 567–574 (1998).
23. Fahrenkopf, N. M. et al. The aim of photonics MPW: a highly accessible cutting-edge technology for rapid prototyping of photonic integrated circuits. *IEEE J. Sel. Top. Quantum Electron.* **25**, 1–6 (2019).
24. Wang, C. et al. Lithium tantalate photonic integrated circuits for volume manufacturing. *Nature* **629**, 784–790 (2024).
25. Pfeiffer, M. H. P. et al. Ultra-smooth silicon nitride waveguides based on the damascene reflow process: fabrication and loss origins. *Optica* **5**, 884–892 (2018).
26. He, L. et al. Low-loss fiber-to-chip interface for lithium niobate photonic integrated circuits. *Opt. Lett.* **44**, 2314–2317 (2019).
27. Gall, D. et al. Electron mean free path in elemental metals. J. Appl. Phys. **119**, 085101 (2016).
28. Harper, J. M. E. et al. Mechanisms for microstructure evolution in electroplated copper thin films near room temperature. *J. Appl. Phys.* **86**, 2516–2525 (1999).
29. Kang, M. S., Kim, S.-K. & Kim, J. J. A novel process to control the surface roughness and resistivity of electroplated cu using thiourea. *Jpn. J. Appl. Phys.* **44**, 8107 (2005).
30. Xu, M. et al. High-performance coherent optical modulators based on thin-film lithium niobate platform. *Nat. Commun.* **11**, 3911 (2020).
31. Holzgrafe, J. et al. Relaxation of the electro-optic response in thin-film lithium niobate modulators. *Opt. Express* **32**, 3619–3631 (2024).
32. Ivanov, M. et al. On the information loss of the max-log approximation in BICM systems. *IEEE Trans. Inf. Theory* **62**, 3011–3025 (2016).
33. Hu, Q. et al. Ultrahigh-net-bitrate 363 gbit/s PAM-8 and 279 gbit/s polybinary optical transmission using plasmonic Mach-Zehnder modulator. *J. Light. Technol.* **40**, 3338–3346 (2022).
34. Berikaa, E. et al. Tfln mzms and next-gen dacs: Enabling beyond 400 gbps imdd o-band and c-band transmission. *IEEE Photonics Technol. Lett.* **35**, 850–853 (2023).
35. Wooten, E. L. et al. A review of lithium niobate modulators for fiber-optic communications systems. *IEEE J. Sel. Top. Quantum Electron.* **6**, 69–82 (2000).
36. Noguchi, K., Mitomi, O. & Miyazawa, H. Millimeter-wave ti: Linbo3 optical modulators. *J. Lightwave Technol.* **16**, 615 (1998).
37. Wang, Y. & Alford, T. Formation of aluminum oxynitride diffusion barriers for Ag metallization. *Appl. Phys. Lett.* **74**, 52–54 (1999).
38. Gao, L. et al. Thermal stability of titanium nitride diffusion barrier films for advanced silver interconnects. *Microelectron. Eng.* **76**, 76–81 (2004).

39. Tang, Y. et al. High-performance thin-film lithium niobate modulator on silicon substrate with a thick silica buffer layer. *Opt. Express* **33**, 20334–20344 (2025).
40. Ohyama, M. et al. Evaluation of hybrid bonding technology of single-micron pitch with planar structure for 3d interconnection. *Microelectron. Reliab.* **59**, 134–139 (2016).
41. Edelstein, D. et al. A high-performance liner for copper damascene interconnects. In *Proceedings of the IEEE 2001 International Interconnect Technology Conference. (Cat. No.01EX461)*, 9–11 (2001).
42. IEEE standard for Ethernet - Amendment 10: Media Access Control Parameters, Physical Layers, and Management Parameters for 200 gb/s and 400 gb/s operation. IEEE Std 802.3bs-201 (2017).

Acknowledgments

We thank Mohammad Bereyhi for helpful discussions. The samples were fabricated in the EPFL Center of MicroNano Technology (CMi) and the Institute of Physics (IPHYS) cleanroom. This project has received funding from the Horizon Europe EIC transition program under grant No. 101113260 (HDLN), and this work was further supported by the Swiss State Secretariat for Education, Research and Innovation (SERI). This work has received funding from the European Research Council (ERC) under the Horizon Europe research and innovation programme, grant agreement No. 101167540 (ATHENS). This material is also based upon work supported by the Air Force Office of Scientific Research under award no. FA8655-24-1-7007.

Author contributions

J.R. conceived the concept. M.L. and Z.L. developed the copper Damascene fabrication process. M.L. designed and fabricated the devices with help from Z.L. and Y.Z. M.L., A.K., H.L., and N.K. performed the measurements and analyzed the data. J.S. and S.Z. carried out device packaging. M.L., A.K., H.L., and T.J.K. wrote the manuscript with input from all authors. C.K. and T.J.K. supervised the project.

Competing interests

TJK is the co-founder of LUXTELLIGENCE SA, offering electro-optical photonic integrated circuits. The other authors declare no competing interests.

Additional information

Supplementary information The online version contains supplementary material available at https://doi.org/10.1038/s41467-026-69588-6.

Correspondence and requests for materials should be addressed to Tobias J. Kippenberg.

Peer review information *Nature Communications* thanks Yikai Su and the other anonymous reviewer(s) for their contribution to the peer review of this work. A peer review file is available.